ELSEVIER

Novel spacers for mass transfer enhancement in membrane separations

F. Li*, W. Meindersma, A.B. de Haan, T. Reith

University of Twente, Faculty of Science and Technology, P.O. Box 217, 7500 AE Enschede, The Netherlands

Abstract

The optimal flow pattern for mass transfer enhancement in spacer-filled channels is characterized by the coexistence of transversal and longitudinal vortices in the flow close to the channel walls and minimal cross-flow power consumption in the middle of the channel. The mass transfer enhancement of spacers with modified filaments, twisted tapes and multi-layer structures, which were expected to generate these flow patterns, was investigated experimentally. The results indicate that the performance of spacers with modified filaments and twisted tapes is generally worse while the performance of spacers with multi-layer structure is generally better than that of the optimal non-woven net spacer. An optimal multi-layer spacer was designed with optimal non-woven nets in the outer layers and twisted tapes in the middle-layer. Its average Sherwood number is about 30% higher than the Sherwood number of the optimal non-woven spacer at the same cross-flow power consumption whereas the cross-flow power consumption is only about 40% of the consumption of the optimal non-woven spacer at the same Sherwood number. The Reynolds number based on the height of a spacer-filled channel varies from 40 to 500 in present study.
© 2005 Elsevier B.V. All rights reserved.

Keywords: Membrane filtration; Flow pattern; Novel spacer development; CFD; Limiting current method

1. Introduction

Different techniques of mass transfer enhancement are applied in membrane processes. In general, mass transfer enhancement techniques can be classified either as passive, which require no direct application of external power, or as active, which require external power such as electrical fields, ultrasonic fields and etc. The common enhancement techniques in membrane processes are given in Table 1. In some applications, two or more of the techniques may be utilized simultaneously to produce an enhancement that is larger than the individual techniques applied separately.

In membrane modules, woven and non-woven spacers are often used to enhance mass transfer. The performance of non-woven feed spacers in terms of mass transfer enhancement and energy dissipation has been studied experimentally in the past decades [4,12,13]. Since the late 90 s, computational fluid dynamics (CFD) has been used to investigate the flow

phenomena in more depth in flat channels equipped with spacers [14–16].

In earlier papers of the present authors, the optimization of non-woven spacers in terms of mass transfer (Sh) and cross-flow power consumption (Pn) has been studied by CFD simulations [14] and by experiments [17]. The optimal non-woven spacer geometry was found. The performance of this optimal non-woven spacer is used as a reference against which performance of new spacer geometries is evaluated.

The present study is focused on the development of novel feed spacers in membrane modules, which have a higher mass transfer enhancement than the optimal non-woven spacer. The optimization approach in Sh vs. Pn plots, which has been discussed earlier [14,17], is also used in present study. The development of the novel spacer is carried out in the following three steps:

(1) Identify the optimal flow pattern for mass transfer enhancement.
(2) Identify spacer geometries and structures which generate the optimal flow pattern.

* Corresponding author. Tel.: +31 53 489 3564; fax: +31 53 489 3663.
  E-mail address: f.li@ctw.utwente.nl (F. Li).

Table 1
Classification of common enhancement techniques

Passive techniques	Active techniques
Spacers [1,2]	Surface vibration [11]
Corrugated membrane surfaces [4,10]	Flow vibration [5–7]
Swirling flow devices [3,8]	Ultrasound field [9]

(3) Validate the performance of the novel optimal spacer by experiments.

2. Flow patterns and spacer geometries

2.1. Coexistence of longitudinal and transversal vortices in non-woven spacer-filled channels

Studies on heat transfer enhancement by obstacles in heat exchangers are of interest for the investigation of mass transfer enhancement by spacers in channels, because of the similarity between mass and heat transfer. Many studies have been published on heat transfer enhancement by obstacles in channels of which a small selection [18–32] will be discussed below. Especially the relationship between obstacle geometry, type of flow and heat transfer enhancement is of interest.

Two well-known enhancement mechanisms of heat transfer are: (1) flow separation caused by obstacles as ribs and corrugations on the channel walls perpendicular to the flow direction, followed by flow re-attachment and development of laminar boundary layers downstream of the obstacle along the wall; and (2) swirling flows consisting of rotating vortices. Two types of swirling flows can be recognized: transversal vortices with the axis perpendicular to the flow direction and longitudinal vortices with the axis parallel to the flow direction as schematically shown in Fig. 1. The above mechanisms may occur simultaneously or consecutively in the same channel.

The performance of transversal vortices induced by ribs and corrugations on heat transfer enhancement depends on the flow hydrodynamics:

(1) When the Reynolds number based on the channel height (Re_h) is small ($Re_h < 100$), Grosse-Gorgemann et al. [27] have concluded that transverse ribs and corrugations, as shown in Fig. 1a, generate slowly rotating transversal vortices, which lead to flow separation, re-attachment and development of hydraulic and heat transfer boundary layers, resulting in enhanced heat transfer, while the vortices themselves do not contribute to heat transfer enhancement. This conclusion has also been substantiated by the work of Fiebig [18] in which it is shown that heat transfer enhancement by flow separation, reattachment and boundary layer development is not efficient when cross-flow power consumption is taken into consideration.

(2) When the Reynolds number (Re_h) is larger than about 150 for the geometry shown in Fig. 1a, a periodic Karman vortex street occurs. The flow is then unsteady and the heat transfer enhancement is mainly due to the time periodic exchange of flow between wall and the flow bulk caused by vortex shedding. For very different geometries,
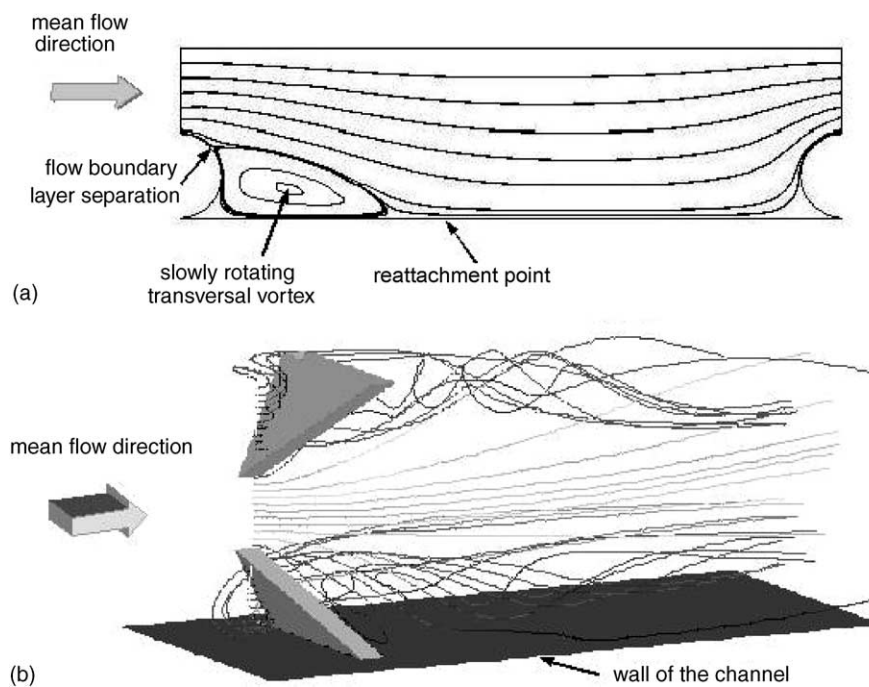

Fig. 1. Swirling flow in flat channels: (a) transversal vortex in a channel with round rods periodically positioned $Re_h = 61$; (b) longitudinal vortices at $Re_h = 374$ induced by delta wings mounted on the flat walls (the upper wall is not shown for the reasons of clarity).

Amon and Mikic [28] and Grosse-Gorgemann et al. [29] have shown that periodic shedding of transversal vortices in ribbed channels cause heat transfer coefficients several times larger than those in an empty channel for the same pumping power. The CFD study by Esfahani [34] shows, that in a flat channel with a square rib attached on one wall, a periodic flow field exists which is two-dimensional in time and space up to a certain Reynolds number ($Re_h \cong 500$). Beyond this Reynolds number, three-dimensional disturbances are amplified leading to the onset of turbulence.

It is concluded from the above discussions that heat transfer enhancement by transversal vortices is most energy-efficient in the Reynolds number range $150 < Re_h < 500$, where vortex shedding occurs. Below this Reynolds range there is no vortex shedding, while above this range turbulence occurs with extremely high cross-flow power consumptions.

Longitudinal vortices can be generated by various types of wings (see Fig. 1b), ribs as shown in Fig. 2, and other geometries such as spacers with appropriate geometric parameters. Fiebig [18] observed that generation of longitudinal vortices leads to the con-occurrence of transversal vortices. They investigated experimentally the joint influence of longitudinal and transversal vortices on heat transfer enhancement in flows generated by a pair of ribs according to Fig. 2, of which the flow attack angle (θ) can be changed. By pivoting the ribs to $\theta = 90°$, they are transversal vortex generators. Their work shows that for $\theta < 60°$, the flow is dominated by longitudinal vortices, while for $\theta > 70°$, the flow is dominated by transversal vortices. Optimal heat transfer enhancement was noted at $\theta \cong 65°$. This suggests that an optimal flow pattern is characterized by the coexistence of longitudinal and transversal vortices. Although Fiebig [18] carried out their studies in the Reynolds range $500 < Re_h < 4000$, which is outside the range of the present paper, it is believed that these results can be extrapolated to the range $100 < Re_h < 500$.

In order to demonstrate the applicability of the above results of Fiebig [18] to non-woven spacers, CFD velocity calculations were carried out for three non-woven spacer geometries. The geometric parameters (α, β and l/h) characterizing the non-woven spacer geometry are illustrated in Fig. 3. The optimal non-woven spacer has the geometric parameters $\alpha = 30°$, $\beta = 120°$, $l/h = 4$ [14,17]. The three spacers are:

(1) The non-woven spacer with $\alpha = 60°$, $\beta = 60°$, $l/h = 4$ ($Re_h = 296$) in Fig. 4;
(2) The non-woven-spacer with $\alpha = 0°$, $\beta = 90°$, $l/h = 4$ ($Re_h = 188$) in Fig. 5.
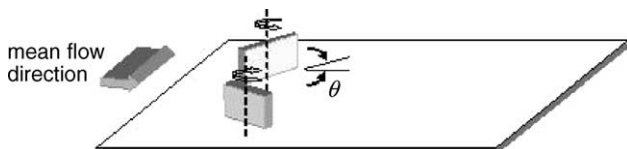

Fig. 2. A pair of ribs mounted on flat wall with adjustable flow attack angle.

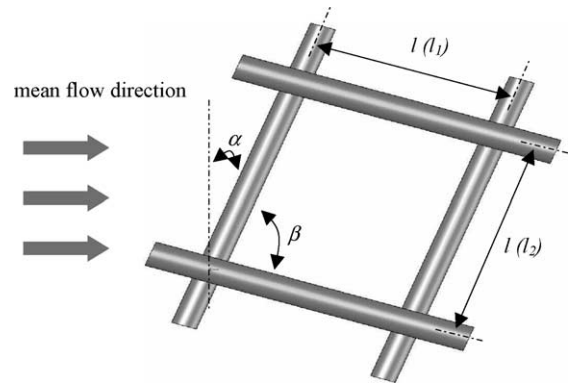
Fig. 3. Geometric characterization of a commercial non-woven spacer.

(3) The optimal non-woven spacer with $\alpha = 30°$, $\beta = 120°$, $l/h = 4$ ($Re_h = 122$) in Fig. 6.

The velocity components were calculated in plane(s) as sketched schematically in Figs. 4a, 5a and 6a and shown in the velocity plots in Figs. 4b, 4c, 5b, 6b and 6c. The following velocities were chosen:

- Velocities in plane 1, which is perpendicular to the channel wall and parallel to the mean flow direction. When a local velocity pattern indicating a rotating liquid mass can be seen in the vector plot, a transversal vortex is present there.
- Velocities in plane 2, which is perpendicular to the channel wall and the mean flow direction. When a local velocity pattern indicating a rotating liquid mass can be seen in the vector plot, a longitudinal vortex is present there.

Three longitudinal vortices are present in the spacer shown in Fig. 4. The spacer in Fig. 5 exhibits only one transversal vortex. For that reason only the velocity vector plot in a plane perpendicular to the mean flow direction is shown. The coexistence of one longitudinal and two transversal vortices in the optimal spacer is obvious in Fig. 6. In the previous publications by the authors [14,17] it was shown that the latter spacer is indeed optimal, confirming the observations of Fiebig [18] for larger Reynolds numbers.

2.2. The optimal flow pattern for mass transfer enhancement in spacer-filled flat channels

Not only the coexistence of longitudinal and transversal vortices is essential, but also the spatial distribution of the vortices in a spacer is of great importance for the optimal spacer performance. Figs. 4–6 show that the vortices in non-woven spacers occur mainly in the bulk of the flow. Since the resistance against mass transfer from the bulk of the flow to the wall of the channel is situated in the immediate vicinity of the wall, mass transfer enhancement in the bulk of the flow can not be energy-effective. The obvious conclusion is that vortices should be generated close to the channel wall.
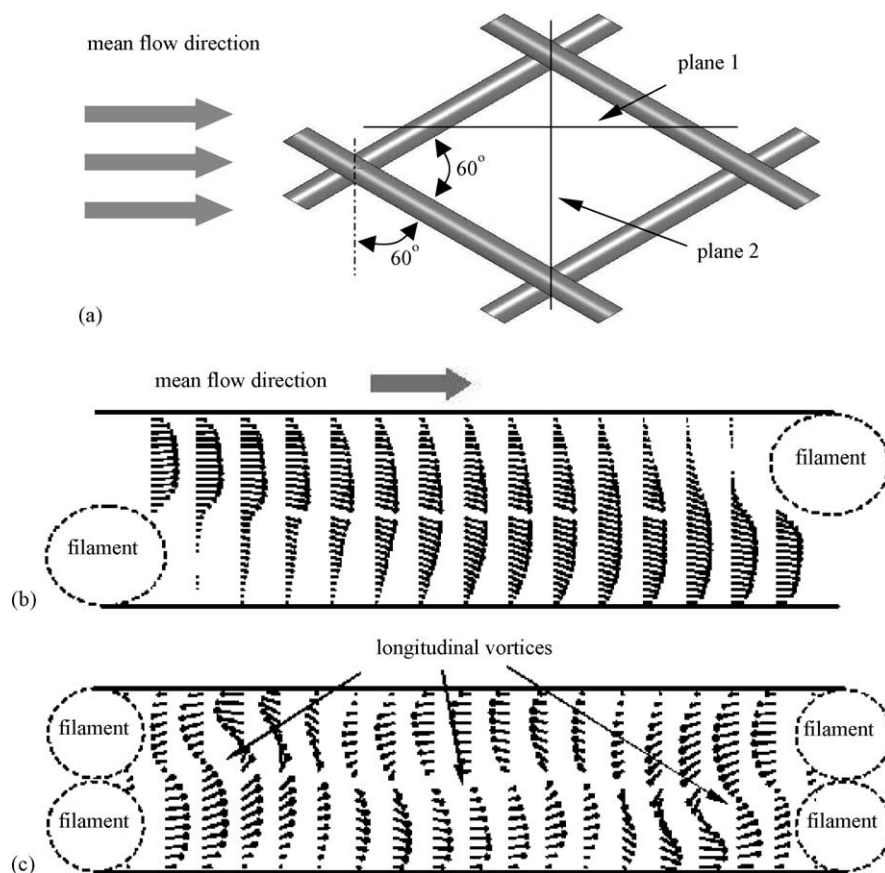
Fig. 4. Vector plots for a non-woven spacer with $\alpha = 60°$, $\beta = 60°$, $l/h = 4$ ($Re_h = 296$): (a) the position of the planes 1 and 2; (b) the vector plot of velocities in plane 1; (c) the vector plot of velocities in plane 2.

From the above deliberations, it can be concluded that the optimal flow pattern in terms of mass transfer enhancement and cross-flow power consumption should have the following characteristics:

(1) Coexistence of longitudinal and transversal vortices in the flow close to the channel walls.
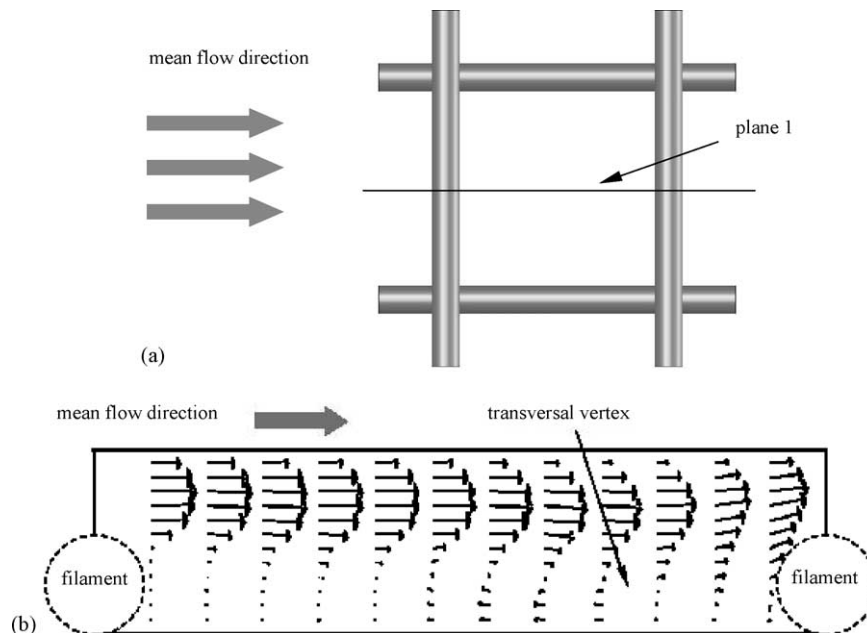(2) Minimal cross-flow power consumption in the middle of the flow channel.

Fig. 5. Vector plot for a non-woven spacer with $\alpha = 0°$, $\beta = 90°$, $l/h = 4$ ($Re_h = 188$): (a) the position of plane 1; (b) the vector plot of velocities in plane 1.
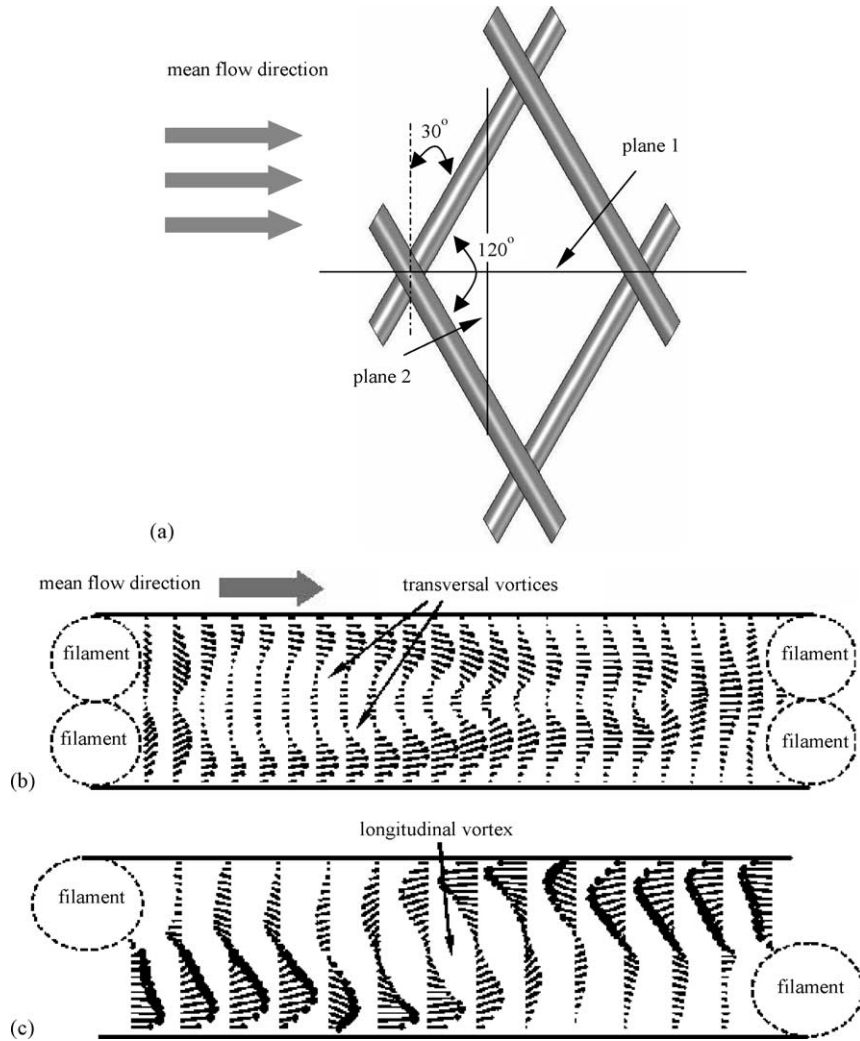
Fig. 6. Vector plots for the non-woven spacer with $\alpha = 30°$, $\beta = 120°$, $l/h = 4$ ($Re_h = 122$): (a) the position of the planes 1 and 2; (b) the vector plot of velocities in plane 1; (c) the vector plot of velocities in plane 2.

One way to bring the vortices closer to the wall would be to fix non-woven spacers with small filament diameters on the walls of the channel, thereby leaving the major part of the cross section of the channel open for the bulk of the flow. This idea is checked experimentally by comparing the performance of the usual non-woven spacer with filament diameters $d = h/2$ with that of a non-woven spacer with smaller diameters $d = h/12$. The latter, thinner, spacer is placed on the top and bottom walls of the flat channel, leaving the middle part of the channel open. Fig. 7 shows the poorer performance of the thinner spacer at low Reynolds (and power) numbers. A plausible explanation is that the flow phenomena near the spacer filaments are governed by the local Reynolds numbers, which are dependent on the filament diameter. Since the local Reynolds numbers for the thinner spacer are much smaller than those for the usual spacer, the mass transfer enhancing mechanisms described in Section 2.1 occur at larger superficial velocities and cross-flow power consumptions in the thinner spacer.
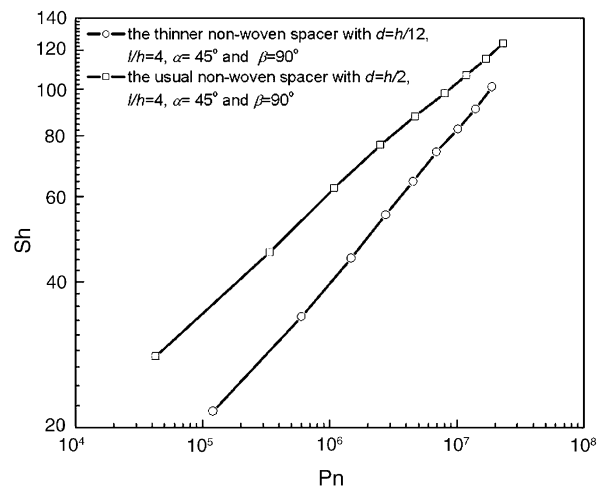
Fig. 7. Comparison of the experimental results obtained with the usual non-woven spacer with $d = h/2$ and a thinner non-woven spacer with $d = h/12$.

The above considerations and experimental investigation indicate that, in order to create the required mix of longitudinal and transversal vortices close to the wall and to minimize the cross-flow power consumption in the middle of the channel, appropriate spacers have to be developed.

2.3. Spacer geometries to be investigated

The performance of the following spacer geometries was investigated:

(1) Spacers with modified filaments as shown in Fig. 8 (1). The modified filament has a helical bar winding around the cylindrical filament. It is expected that this helical winding generates longitudinal vortices close to wall, which effectively enhances mass transfer. In addition to the geometric parameters for non-woven spacers shown

Table 2
Geometric parameters of the MF and TT spacers

No.	h (mm)	l/h	α (°)	β (°)	n	D/h	D_i/h	D_o/h	t/h
MF	4	4	45	90	2	–	0.34	0.50	0.13
TT	4	4	45	90	1	0.5	–	–	0.13

in Fig. 3, the following geometric parameters are required: the 360° twist pitch (w), the thickness of helical rods (t), the inner diameter (D_i) and the outer diameter (D_o). These parameters are made dimensionless by division by h. The ratio of w/h is also referred to as the twist ratio (n). All geometric parameters are shown in Table 2.

(2) Twisted tapes as shown in Fig. 8(2). Twisted tapes have been extensively used in heat transfer enhancements [30]. In those applications, the twisted tape inserts in heat exchangers parallel to the main flow direction are used to generate swirling flow. Investigations of the performance
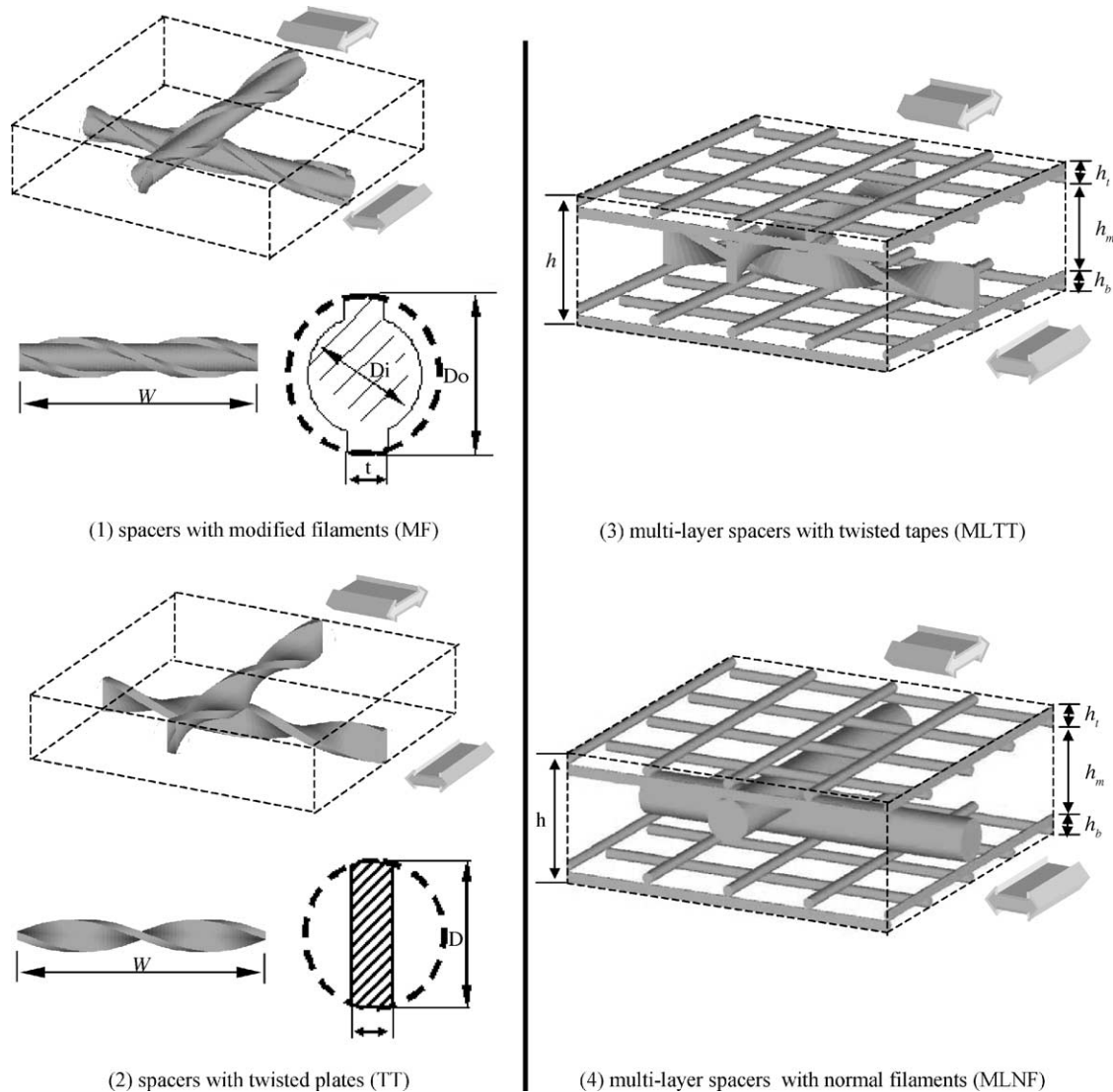

(1) spacers with modified filaments (MF)

(2) spacers with twisted plates (TT)

(3) multi-layer spacers with twisted tapes (MLTT)

(4) multi-layer spacers with normal filaments (MLNF)

Fig. 8. Geometric configuration of novel spacers.

Table 3
Geometric parameters of multi-layer spacers

No.	Layers	Type	h_i[a] (mm)	h_i/h[a]	l_i/h_i[a]	α (°)	β (°)	D/h_i[a]	t/h_i[a]	n
MLNF1	Top	Non-woven	1	0.17	4.0	30	120	0.5	–	–
	Middle	Non-woven	4	0.66	4.0	30	120	0.5	–	–
	Bottom	Non-woven	1	0.17	4.0	30	120	0.5	–	–
MLNF2	Top	Non-woven	1	0.17	4.0	45	90	0.5	–	–
	Middle	Non-woven	4	0.66	4.0	45	90	0.5	–	–
	Bottom	Non-woven	1	0.17	4.0	45	90	0.5	–	–
MLTT1	Top	Non-woven	1	0.17	4.0	45	90	0.5	–	–
	Middle	Twisted plates	4	0.66	4.0	45	90	0.5	0.13	1
	Bottom	Non-woven	1	0.17	4.0	45	90	0.5	–	–

[a] the subscript i represents either t (for the top layer), m (for the middle layer) or b (for the bottom layer) where appropriate.

of twisted tapes in viscous process fluids have shown that the relative heat transfer enhancements in laminar flow region are substantially greater than that in turbulent flows [30–32]. One may expect a similar behavior in the area of mass transfer. In addition to the geometric parameters shown in Fig. 3, the dimensionless parameters for geometric characterization are required: the twist ratio (n) and the thickness of twisted tapes (t). All geometric parameters are listed in Table 2.

(3) The performance of spacers with multi-layer structures is investigated with the spacers shown in Fig. 8(3) and (4). These multi-layer spacers have three distinct layers. The layers close to the channel walls generate swirling flows, and the middle layer diverts the flow from bulk to the channel walls. The geometric parameters needed for characterization of multi-layer structures are the height of each layer (h_t for the top layer, h_m for the middle layer, and h_b for the bottom layer) as shown in Fig. 8 (3) and Fig. 8 (4) leading to the dimensionless parameter h_t/h, h_m/h, and h_b/h, the usual geometric parameters for non-woven spacers (α, β, l_t/h_t, l_m/h_m, l_b/h_b), and the additional geometric parameters for twisted tapes in case they are adopted in the multi-layer spacers. All geometric parameters are shown in Table 3.

The first two spacer geometries with modified filaments and tapes are derived from the non-woven net spacers discussed earlier. Since they do not necessarily satisfy the criterion of minimal power consumption in the middle of the channel, a novel inhomogeneous spacer is studied having a middle layer.

The reader is referred to earlier publications of the authors [14,17] for a more detailed discussion on the use of dimensionless geometric parameters.

3. Numerical and experimental studies

3.1. Summary of the theory

Mass transfer and cross-flow power consumption in geometrically similar spacers is described by dimensional anal-

ysis as shown by the authors in a previous paper [14]. The results are summarized by Eq. (1):

$$Sh = F(Pn, Sc, \lambda_1 \ldots \lambda_m) \tag{1}$$

The m dimensionless geometric parameters are indicated by $\lambda_1 \ldots \lambda_m$. The physical quantities in Eq. (1) are defined below.

The local mass transfer coefficient is defined as:

$$k \equiv \frac{1}{C_b - C_w}\left(-D\frac{\partial C}{\partial y}\right)_{\text{wall}} \tag{2}$$

The mass transfer coefficient averaged over the area of both channel walls is:

$$k_m = \frac{1}{A}\int_A k \, dA \tag{3}$$

The (average) Sherwood number is then:

$$Sh \equiv \frac{k_m h}{\mathcal{D}} \tag{4}$$

Furthermore the Schmidt number is: $Sc \equiv \mu/\rho\mathcal{D}$ and the power number is: $Pn = \text{SPC } \rho^2 h^4/\mu^3$, with the cross flow power consumption per unit volume of spacer-filled channel: $\text{SPC} \equiv \Delta P u w h/L w h = \Delta P u/L$.

Evaluation of spacer performance and optimization of spacer geometry is based on the comparison of two parameters: the consumption of cross-flow mechanical (pumping) power per unit volume of spacer SPC and the product of mass transfer coefficient and mass transfer area (wall or membrane area) per unit volume of spacer SKA. Spacers with a higher SKA per SPC are more efficient. In order to facilitate this comparison, the parameters SKA and SPC are incorporated in the dimensionless Sherwood numbers Sh and power numbers Pn, respectively: $Sh \equiv k_m h/\mathcal{D} = k_m L w h^2/L w h \mathcal{D} = \text{SKA } h^2/\mathcal{D}$ and $Pn = \text{SPC } \rho^2 h^4/\mu^3$.

The performance of a spacer is characterized by its position in a Sh versus Pn plot.

3.2. CFD simulation

Flow patterns and mass transfer in spacers are calculated by the commercial CFD package CFX-4. An overview of
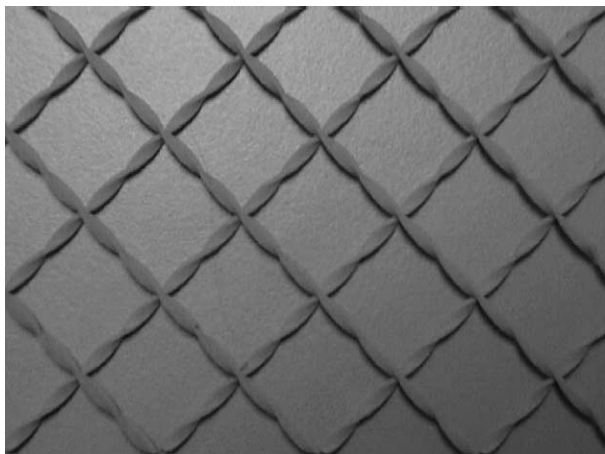
Fig. 9. The TT spacer manufactured by SLS technology.

Fig. 10. Comparison of the MF spacer, TT spacer and optimal non-woven spacer.

the models and calculation procedures has been given in an earlier paper of the present authors [14].

3.3. The manufacturing technique of spacers

The novel spacers used for the experimental investigations were manufactured with the Selective Laser Sintering (SLS) technology. For detailed information about this technology, the reader is referred to the literature [33]. An important step is the preparation of the 3D CAD model of the spacer, which is then used to control the SLS machine. Fig. 9 shows the spacer with twisted tapes manufactured with SLS technology.

3.4. Experimental

The limiting current method is used to obtain the mass transfer coefficients on the walls of spacer-filled channels. All experiments are conducted at $20 \pm 0.2\,°C$ and the Schmidt number is $Sc = 1.28 \times 10^3$. For detailed information of the method and the set-up used in the study, the reader is referred to the previous paper of the present authors [17].

4. Results and discussions

4.1. Spacers with modified filaments (MF) and twisted tapes (TT)

The spacers with modified filaments MF and twisted tapes TT are compared in Fig. 10. The CFD simulations (dashed lines) predict a higher performance than actually measured. The explanation is that CFD simulations for spacers with complicated geometries lead to numerical inaccuracies. See for a more detailed analysis of calculation errors in the CFX-4 software the doctoral thesis of Li [35]. Therefore, the comparison between the MF and TT spacers is based on experimental results only.

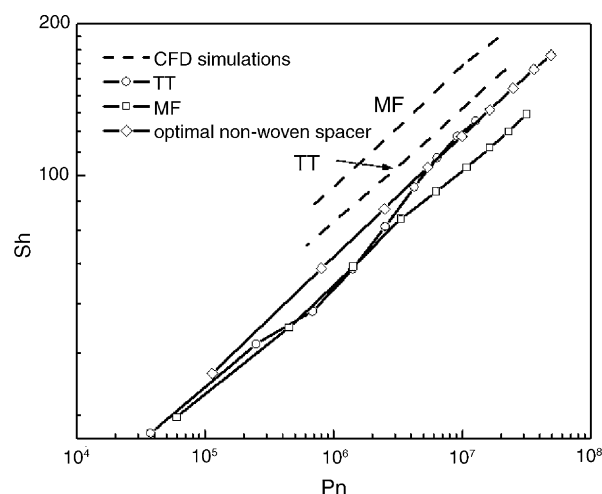The flow patterns in the velocity vector plots in Fig. 11 for the MF spacer and in Fig. 12 for the TT1 spacer are both dominated by longitudinal vortices in the middle of the channel, which do not contribute to spacer performance. It is hardly surprising that the MF and TT spacers are inferior to the optimal non-woven spacer.

4.2. Spacers with multi-layer structures

Since the geometries of multi-layer spacers are even more complicated than those of the MF and TT spacers (see Fig. 8) mass transfer simulations in these spacers by CFD can not be reliable. Therefore, there was no point in carrying out the extremely time-consuming generation of numerical grids for the computational domain. Only experiments were used to study the performance of multi-layer spacers.

Three multi-layer spacers were investigated experimentally:

- the MLNF1 spacer having the same geometric parameters ($\alpha = 30°$, $\beta = 120°$ and $l_i/h_i = 4$) as the optimal non-woven spacer,
- the MLFN 2 spacer with the sub-optimal non-woven spacer geometry ($\alpha = 45°$, $\beta = 90°$ and $l_i/h_i = 4$), and
- the MLTT1 spacer with a middle layer consisting of twisted tapes.

Full details of the spacer geometries are shown in Fig. 8 and Table 3.

The performance of the three multi-layer spacers is presented in Fig. 13 and compared with that of the optimal non-woven spacer. For a better understanding of the results, also the power consumptions in Fig. 14 should be consulted.

The figure shows clearly that the MLNF1 spacer with the optimal non-woven spacer geometry does not perform better than the MLFN 2 spacer. This is a consequence of the higher power consumption in the MLFN1 spacer, as shown in Fig. 14. But it is also clear that the performance of the
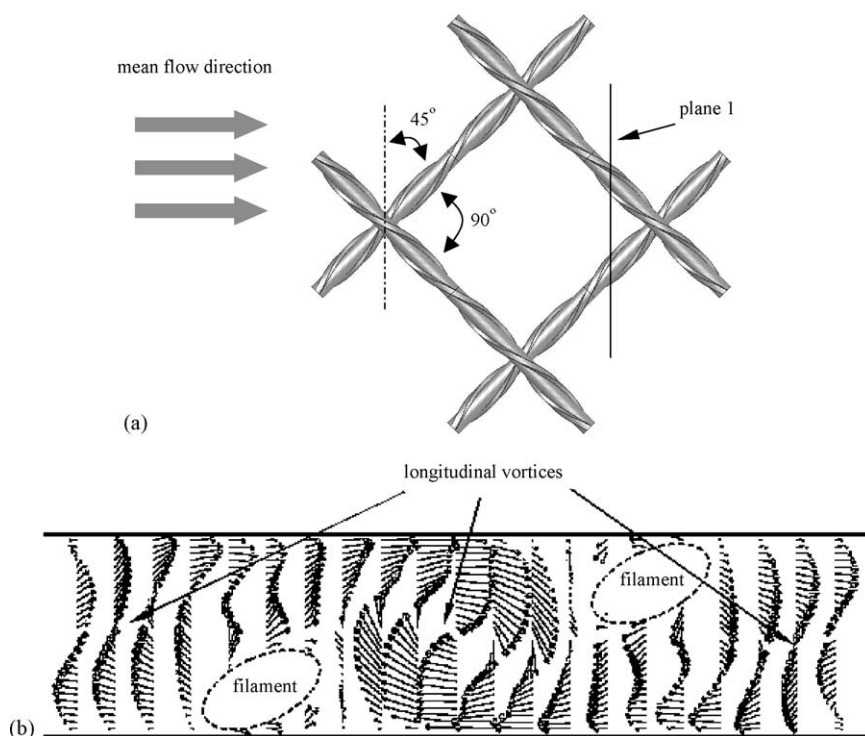
Fig. 11. Longitudinal vortices in a flat channel filled with MF spacer at $Re_h = 371$: (a) the position of plane 1; (b) the vector plot of velocities in plane 1. (The position of the filament cross-section is indicated by ovals in this figure.)

MLNF1 and MLNF2 spacers is only slightly better than the optimal non-woven spacer. The salient role of the middle layer in improving the performance of multi-layer spacers can be deducted from the comparison of the MLNF1 and MLNF2 spacers with the better performing MLTT1 spacer. The superior performance of MLTT1 spacer results mainly from the lower power dissipation in the twisted tapes situated in the middle layer.
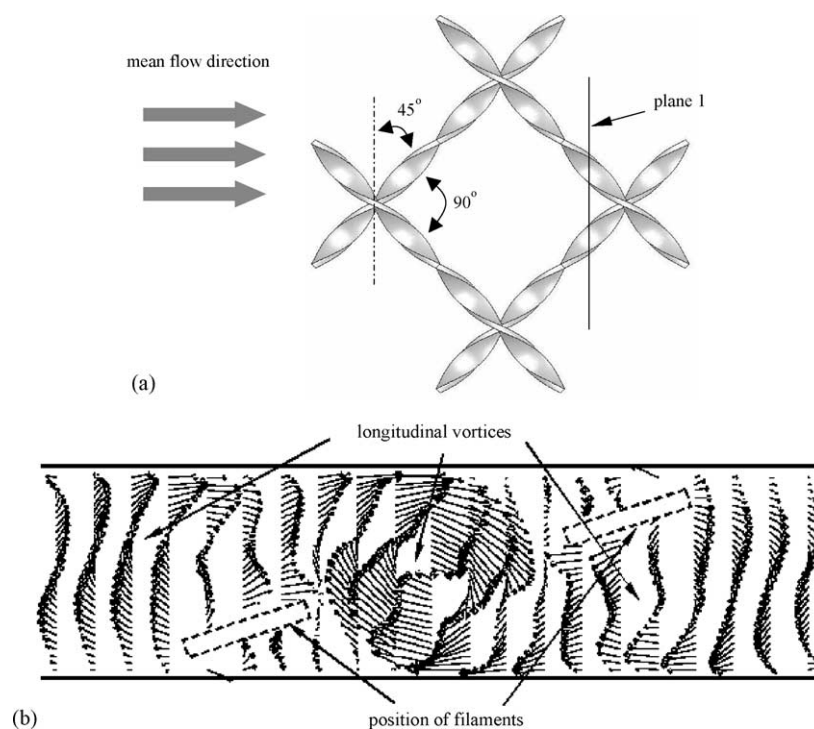

Fig. 12. Longitudinal vortices in the channel filled with TT spacer at $Re_h = 321$: (a) the position of plane 1; (b) the vector plot of velocities in plane 1. (The position of the filament cross-section is indicated by the rectangles in this figure.)

Table 4
Geometric parameters of the optimal multi-layer spacer

	Type	h_i^a (mm)	h_i/h^a	l_i/h_i^a	α (°)	β (°)	D/h_i^a	t/h_i^a	n
Top layer	Non-woven	1	0.17	4.0	30	120	0.5	–	–
Middle layer	Twisted plates	4	0.66	4.0	30	120	0.5	0.13	1
Bottom layer	Non-woven	1	0.17	4.0	30	120	0.5	–	–

[a] the subscript i represents either t (for the top layer), m (for the middle layer) or b (for the bottom layer) where appropriate.
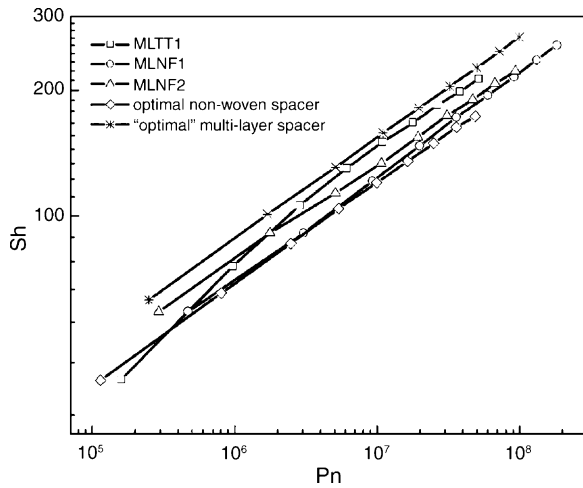

Fig. 13. Comparison of multi-layer spacers.

4.3. The optimal high performance spacer with multi-layer structure

The MLTT1 spacer is further optimized by modifying the geometrical parameters of the two non-woven layers from $\alpha = 45°$, $\beta = 90°$, $l_i/h_i = 4$ into $\alpha = 30°$, $\beta = 120°$, $l_i/h_i = 4$, i.e. the geometrical parameters of the optimal non-woven spacer, as shown in Table 4.

The performance of this spacer is presented in Fig. 13. Comparison of this spacer with the optimal non-woven spacer and the multi-layer spacers discussed earlier indicates that the

Fig. 14. Relation between Power numbers and Reynolds numbers.

performance of this multi-layer spacer is very promising. Its average Sherwood number is about 30% higher than that of the optimal non-woven spacer at the same cross-flow power consumption whereas the cross-flow power consumption is only about 40% of the optimal non-woven spacer at the same average Sherwood number.

It can be seen from the plot of Pn versus Re in Fig. 14 that the measurements have been executed in the Reynolds number range 40–500.

It should be pointed out here that, due to the limited number of multi-layer spacers studied in this research, the possibility can not be ruled out that a more efficient multi-layer spacer can be identified by varying its geometrical parameters. However, the present optimal multi-layer spacer appeared to be already so promising that a patent application has been filed [36].

5. Conclusions

CFD simulations of the mass transfer in spacers with intricate geometries as modified filaments, twisted tapes and multi-layer structures are unreliable. In this study the comparison of mass transfer in spacer-filled channels has been based purely on experiments.

The optimal flow pattern in spacer-filled channels is characterized by the coexistence of transversal and longitudinal vortices.

The performance of both modified filaments and twisted tapes is inferior to the optimal non-woven spacer.

The performance of multi-layer spacers is equal or superior to that of the optimal non-woven spacer. The spacers with a twisted tape middle-layer are most effective.

Finally, the novel optimal multi-layer spacer with optimal non-woven nets in the outer layers and twisted tapes in the middle-layer is identified as the best performing spacer. Its average Sherwood number is about 30% higher than that of the optimal non-woven spacer at the same cross-flow power consumption whereas the cross-flow power consumption is only about 40% of the optimal non-woven spacer at the same average Sherwood number.
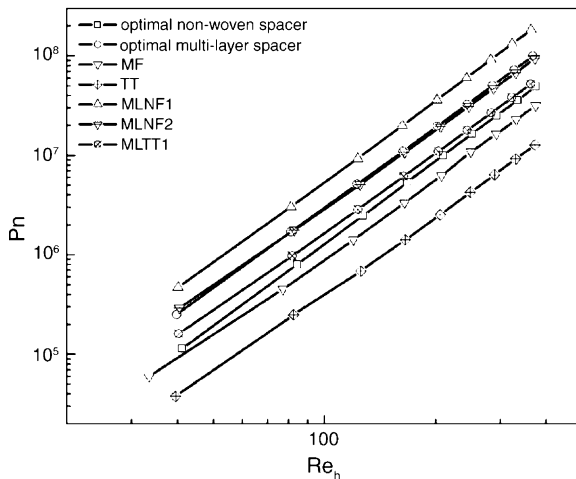
Nomenclature

A	total area of both channel walls (m^2)
C_b	bulk concentration (M)
C_w	concentration at channel wall surfaces (M)
d	filament diameter
$\mathcal{D}$	liquid diffusivity (m^2/s)
h	channel height (m)
h_t	thickness of the top layer in the multi-layer spacer (m)
h_m	thickness of the middle layer in the multi-layer spacer (m)
h_b	thickness of the bottom layer in the multi-layer spacer (m)
k	local mass transfer coefficient (m/s)
k_m	average mass transfer coefficient (m/s)
l	filament spacing (m)
l_1	filament spacing (m)
l_2	filament spacing (m)
l_t	filament spacing of the top layer in the multi-layer spacer (m)
l_m	filament spacing of the middle layer in the multi-layer spacer (m)
l_b	filament spacing of the bottom layer in the multi-layer spacer (m)
L	length of spacer-filled channel (m)
Pn	power number $Pn = \text{SPC} \frac{\rho^2 h^4}{\mu^3}$
Re_h	the Reynolds number $Re_h \equiv \frac{\rho u h}{\mu}$
Sc	Schmidt number $Sc \equiv \frac{\mu}{\rho \mathcal{D}}$
Sh	Sherwood number averaged over both channel walls $Sh \equiv \frac{k_m h}{\mathcal{D}}$
SKA	product of average mass transfer coefficient and wall area per unit volume of spacer, $\text{SKA} \equiv \frac{k_m L w}{L w h}$
SPC	specific power consumption in the channel, $\text{SPC} \equiv \frac{\Delta P u w h}{L w h} = \frac{\Delta p}{L} u$
u	superficial velocity in the channel (m/s)
w	channel width (m)

Greek letters

α	flow attack angle
β	angle between crossing filaments
λ	geometric parameter
μ	dynamic viscosity of the solution (Pas)
ρ	density of the solution (kg/m^3)
ΔP	pressure difference over the channel (Pa)

References

[1] A.R. Da Costa, A.G. Fane, D.E. Wiley, Ultrafiltration of whey protein solutions in spacer-filled channels, J. Membr. Sci. 76 (1993) 245–254.

[2] W.G. Light, T.V. Tran, Improvement of thin-channel design for pressure-driven membrane systems, Ind. Eng. Chem. Process Des. Dev. 20 (1981) 33–40.

[3] H.R. Millward, B.J. Bellhouse, G. Walker, Screw-thread flow promoters: an experimental study of ultrafiltration and microfiltration performance, J. Membr. Sci. 106 (1995) 269–279.

[4] M.J. van der Waal, I.G. Racz, Mass transfer in corrugated-plate membrane modules. I. Hyperfiltration experiments, J. Membr. Sci. 40 (1989) 243–260.

[5] H.R. Millward, B.J. Bellhouse, I.J. Sobey, R.W.H. Lewis, Enhancement of plasma filtration using the concept of the vortex wave, J. Membr. Sci. 100 (1995) 121–129.

[6] T. Nishimura, Mass transfer enhancement in a furrowed channel with arc-shaped walls for pulsatile flow, Heat Transer Jpn. Res. 24 (1995) 115–132.

[7] J.A. Howell, R.W. Field, D. Wu, Yeast cell microfiltration: flux enhancement in baffled and pulsatile flow systems, J. Membr. Sci. 80 (1993) 59–71.

[8] H.M. Yeh, K.T. Chen, Improvement of ultrafiltration performance in tubular membranes using a twisted wire-rod assembly, J. Membr. Sci. 178 (2000) 33–45.

[9] X. Chai, T. Kobayashi, N. Fujii, Ultrasound effect on cross-fow filtration of polyacrylonitrile ultrafiltration membranes, J. Membr. Sci. 148 (1998) 129–135.

[10] K. Scott, J. Lobato, Mass transfer characteristics of cross-corrugated membranes, Desalination 146 (2002) 255–258.

[11] W.B. Krantza, R.R. Bilodeaua, M.E. Voorheesb, R.J. Elgas, Use of axial membrane vibrations to enhance mass transfer in a hollow tube oxygenator, J. Membr. Sci. 124 (1997) 283–299.

[12] G. Schock, A. Miquel, Mass transfer and pressure loss in spiral wound modules, Desalination 64 (1987) 339–352.

[13] Y. Winograd, A. Solan, M. Toren, Mass transfer in narrow channels in the presence of turbulence promoters, Desalination 13 (1973) 171–186.

[14] F. Li, W. Meindersma, A.B. de Haan, T. Reith, Optimization of net spacers in spiral wound membrane modules, J. Membr. Sci. 208 (2002) 289–302.

[15] Vitor Geralds, Viriato Semiao, Maria Norberto de Pinho, Flow management in nanofiltration spiral wound modules with ladder-type spacers, J. Membr. Sci. 203 (2002) 87–102.

[16] Z. Cao, D.E. Wiley, A.G. Fane, CFD simulation of net-type turbulence promoters in a narrow channel, J. Membr. Sci. 185 (2001) 157–176.

[17] F. Li, W. Meindersma, A.B. de Haan, T. Reith, Experimental validation of CFD mass transfer simulations in flat channels with nonwoven net spacers, J. Membr. Sci. 232 (2004) 19–30.

[18] M. Fiebig, Vortex generators for compact heat exchangers, J. Enhanced Heat Transfer 2 (1995) 43–61.

[19] C.C. Zimmerer, V. Kottke, Effects of spacer geometry on pressure drop, Mass Transfer, Mixing Behavior and Residence Time Distribution, Desalination 104 (1996) 129–134.

[20] J. Leu, M. Liu, J. Liaw, C. Wang, A numerical investigation of louvered fin-and-tube heat exchangers having circular and oval tube configurations, Int. J. Heat Mass Transfer 44 (2001) 4235–4243.

[21] D.M. Hobbs, P.D. Swanson, F.J. Muzzio, Numerical characterization of low Reynolds number flow in the Kenics static mixer, Chem. Eng. Sci. 53 (1998) 1565–1584.

[22] K. Nakabe, K. Suzuki, K. Inaoka, A. Higashio, J.S. Acton, W. Chen, Generation of longitudinal vortices in internal flows with an inclined impinging jet and enhancement of target plate heat transfer, Int. J. Heat Fluid Flow 19 (1998) 573–581.

[23] D.K. Tafti, G. Wang, W. Lin, Flow transition in a multilouvered fin array, Int. J. Heat Mass Transfer 43 (2000) 901–919.

[24] S.K. Saha, A. Dutta, S.K. Dhal, Friction and heat transfer characteristics of laminar swirl flow through a circular tube fitted with regularly spaced twisted-tape elements, Int. J. Heat Mass Transfer 44 (2001) 4211–4223.

[25] T. Adachi, H. Uehara, Correlation between heat transfer and pressure drop in channels with periodically grooved parts, Int. J. Heat Mass Transfer 44 (2001) 4333–4343.

[26] P.G. Vicente, A. Garcia, A. Viedma, Heat transfer and pressure drop for low Reynolds turbulent flow in helically dimpled tubes, Int. J. Heat Mass Transfer 45 (2002) 543–553.

[27] A. Grosse-Gorgemann, W. Hahn, M. Fiebig, Influence of rib heights on oscillations, heat transfer and pressure drop in laminar channel flow, in: Proceedings of Eurotherm 31 "Vortices and Heat Transfer", Bochum, Germany.

[28] C.H. Amon, B.B. Mikic, Numerical prediction of convective heat and mass transfer in self-sustained oscillatory flows, J. Thermophys. Heat Transfer 4 (1990) 239–246.

[29] A. Grosse-Gorgemann, W. Hahne, M. Fiebig, Self-sustained oscillations: heat transfer and flow losses in laminar channel flow with rectangular vortex generators, in: Proceedings of Eurotherm 31 "Vortices and Heat Transfer", Bochum, Germany.

[30] R.M. Manglik, A.E. Bergles, Swirl flow heat transfer and pressure drop with twisted-tape inserts, Advances in Heat Transfer 36 (2002) 183–266.

[31] R.M. Manglik, A.E. Bergles, Heat transfer and pressure drop correlations for twisted-tape inserts in isothermal tubes. I. Laminar flows, J. Heat Transfer 115 (1993) 881–889.

[32] R.M. Manglik, A.E. Bergles, Heat transfer and pressure drop correlations for twisted-tape inserts in isothermal tubes. II. Transition and turbulent flows, J. Heat Transfer 115 (1993) 890–896.

[33] D.T. Pham, R.S. Gault, A comparison of rapid prototyping technologies, Int. J. Mach. Tools Manuf. 38 (1998) 1257–1287.

[34] A. S. Esfahani, Numerical study of laminar, transitional and turbulent flow past rectangular cylinders, Ph.D. thesis, Chalmers University of Technology, Sweden, 1998.

[35] F. Li, Novel spacers for membrane filtration processes, Ph.D. thesis, University of Twente, The Netherlands, 2003.

[36] F. Li, A.B. de Haan, G.W. Meindersma, T. Reith, Patent application no. 1023742 on June 25th, 2003.